A comparison of horizontal and vertical peak accelerations and velocities recorded by S-net ocean-bottom seismographs in the Japan Trench area with the values recorded by stations on the ground in and around the Kanto Basin

Yadab P Dhakal and Takashi Kunugi

National Research Institute for Earth Science and Disaster Resilience, Tsukuba, Japan

PRESENTED AT:

INTRODUCTION

A large-scale seafloor observation network for earthquake and tsunami, abbreviated as S-net, consisting of 150 observatories in the Japan Trench area, has been operated by National Research Institute for Earth Science and Disaster Resilience (NIED) since 2016 (Aoi et al. 2020). One of the main objectives of the establishment of the S-net was to enhance the Japan Meteorological Agency (JMA) earthquake early warning (EEW) and tsunami early warning (Aoi et al. 2020).

Dhakal et al. (2021) compared horizontal peak ground accelerations (PGAs), peak ground velocities (PGVs), and acceleration response spectra at selected periods between the land and S-net sites for nine selected earthquakes ranging in magnitudes between Mw 5.3 and 7.1. They reported that the ground motions at periods between about 0.5 and 10 s were more prominent at the S-net sites.

In the present study, we compared not only the horizontal component peak amplitudes between the land and S-net sites, but also compared the peak amplitudes of the vertical components. Vertical components are of special interest in the seafloor due to the presence of water layer above. The PGAs and PGVs from the P- and S-wave parts of the vertical components were compared between the land and S-net sites. Data from three earthquakes of Mw 5.8-5.9, which occurred nearby the Kanto Basin, were analyzed. As thick sediment is known to exist beneath the S-net stations in the Japan Trench area, we also compared the PGAs obtained from the 0.1 to 0.5 Hz bandpass-filtered long-duration records between the S-net and land stations in the Kanto Basin. The data and processing are explained in the next section, which are followed by the main results in the latter sections. The details of the results presented in this study and further analysis results about the durations of long-period ground motions can be found in our paper, Dhakal and Kunugi (2021). In this presentation, the example waveform plots are new, and the results are shown in a different and concise way.

DATA AND METHODS

The epicenters of the three earthquakes used in this study are shown in Figure 1, with the focal mechanism plots. The events are labelled as 2018, 2020a, and 2020b, respectively. The 2018 earthquake occurred on July 7, 2018, which had Mw value of 5.9. The 2020a earthquake occurred on January 3, 2020, which had Mw value of 5.8. The 2020b earthquake occurred on June 25, 2020, which had Mw value of 5.9. The Mw values were taken from the F-net moment-tensor catalog by NIED. The Japan Meteorological Agency (JMA) magnitudes of the earthquakes were 6.0, 5.8, and 6.1, respectively. Similarly, the JMA focal depths of the events were 56, 34, and 36 km, respectively. The 2018, 2020a, and 2020b events are classified as intraslab, interplate, and crustal earthquake types based on focal depths estimated by JMA and focal mechanisms and depths estimated by F-net (NIED) moment-tensor solution.

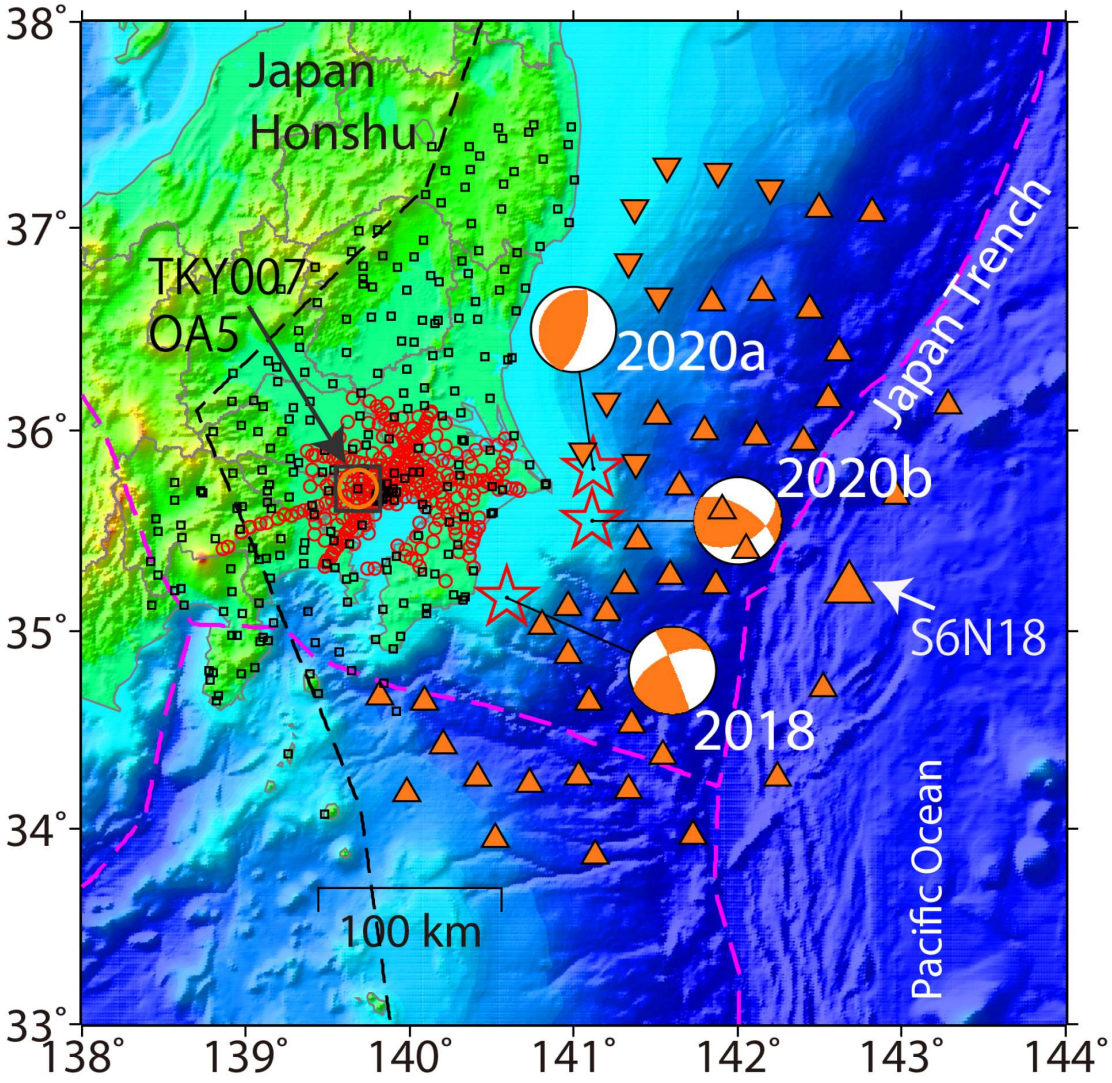

Figure 1 Index map showing location of strong-motion stations and epicenters of earthquakes used in this study. The triangles denote the S-net ocean-bottom stations (inverted triangles denote the buried stations). The squares and circles denote the K-NET/KiK-net and MeSO-net stations, respectively. The stars denote epicenters of the earthquakes. The focal mechanism plots of the earthquakes are connected to the corresponding epicenters by straight lines and are annotated by event codes. The large square, circle, and triangle, pointed by arrows, denote the locations of the sites, namely TKY007 (K-NET), OA5 (MeSO-

net), and S6N18 (S-net), respectively; example waveforms are shown below recorded at the sites. The dashed black line denotes the volcanic front, and the purple lines tectonic boundaries.

The peak amplitude features of S-net records are evaluated with reference to the records from the other three networks, namely, K-NET, KiK-net, and MeSO-net for both horizontal and vertical components of motions. The K-NET and KiK-net are countrywide networks with an average spacing of about 20 km (e.g., Okada et al. 2004, Aoi et al. 2020). The MeSO-net, abbreviated for the Metropolitan Seismic Observation network, is a dense network of about 300 seismometers installed at the borehole depth of 20 m in the Tokyo Metropolitan area (e.g., Sakai and Hirata 2009). The average interstation distance of MeSO-net is about 3 km. The MeSO-net and S-net stations record the waveform data continuously. This means that the long-duration records of an earthquake can be obtained from the S-net and MeSO-net. However, it isn't easy to compare the high-frequency ground motions recorded at the MeSO-net sites with those at the S-net sites because the MeSO-net seismometers are installed at the borehole, as mentioned above. On the other hand, the K-NET seismometers are installed at the ground surface, while the KiK-net consists of a pair of seismometers installed at the ground surface and the borehole. The K-NET and KiK-net stations get triggered after some threshold ground accelerations, and the records get terminated when the threshold motions are not exceeded for a certain duration. Therefore, the S-net records are compared with the K-NET and KiK-net surface records for the high-frequency motions such as the P- and S-wave parts, while the MeSO-net records for the long-period ground motions were used to compare with the S-net records.

The azimuth information about the sensors of S-net stations were taken from Takagi et al. (2019) while those at the MeSO-net were taken from Kano et al. (2015). In the present data set, the rotations of the sensors at the S-net sites were small or negligible due to smaller PGAs, but for the large PGA and PGV sites at near sites, the records should be carefully analyzed (e.g., Nakamura and Hayashimoto 2019, Takagi et al. 2019, Dhakal et al. 2021a).

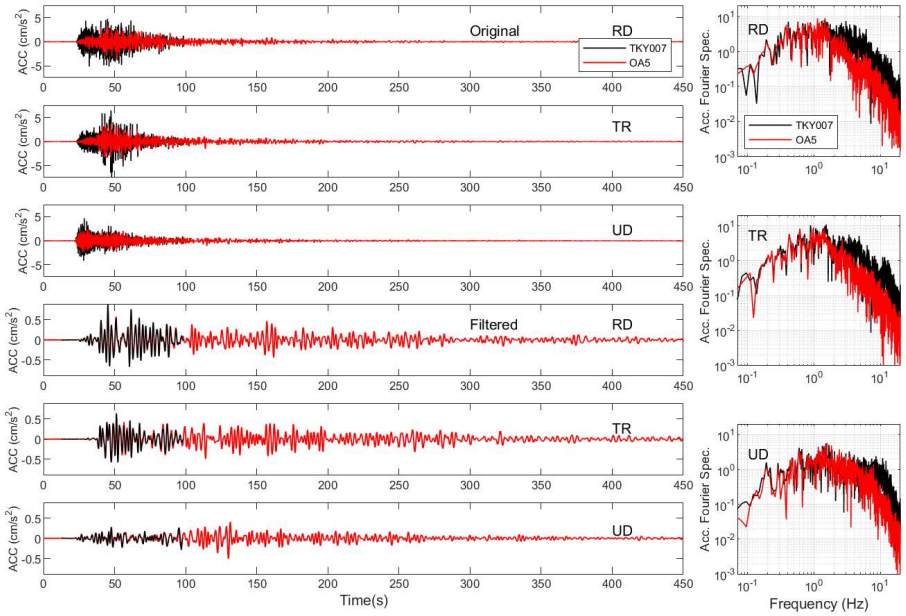

Figure 2 Example acceleration waveforms for the radial (RD), transverse (TR), and vertical (UD) components recorded at the K-NET TKY007 site (black) and MeSO-net OA5 site (red) during the 2020b event (see Figure 1 for the location of the sites and the event). The upper-three left panels show the as-recorded accelerograms rotated to radial, transverse, and vertical components, while the lower-three left panels show the 0.1 to 0.5 Hz bandpass-filtered waveforms. Note that the record length for the K-NET TKY007 site is shorter than that for the MeSO-net OA5 site and is about 100 s. The right panels show the Fourier spectra for the RD, TR, and UD components, respectively, computed for the identical record length of about 100 s. The sites were located about 135 km far from the epicenter of the 2020b event.

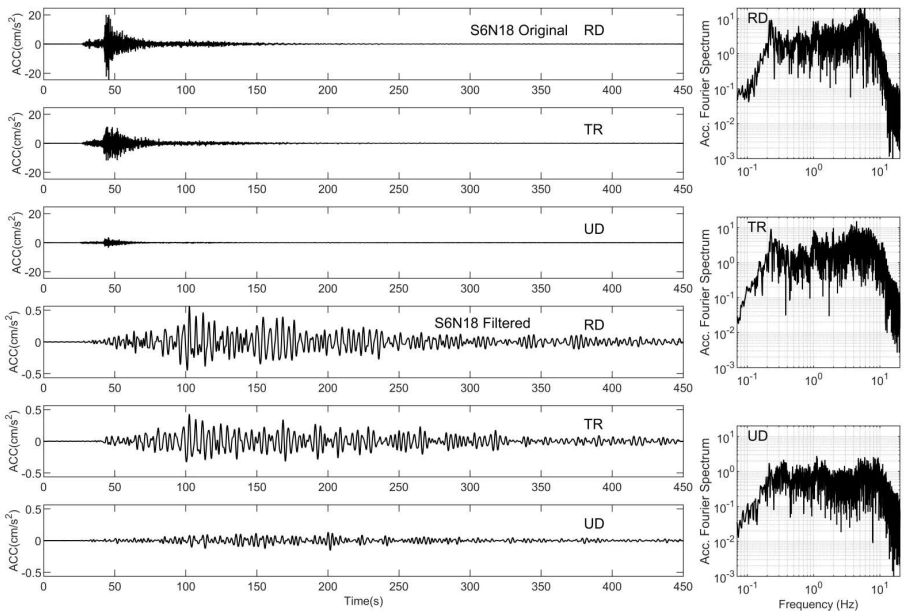

Figure 3 Example acceleration waveforms for the radial (RD), transverse (TR), and vertical (UD) components recorded at the S-net S6N18 site during the 2020b event (see Figure 1 for the location of the site). The upper three left panels show the waveforms without filtering, while the lower three left panels show the 0.1 to 0.5 Hz bandpass-filtered waveforms. The right panels show the acceleration Fourier spectra for the RD, TR, and UD components, respectively, computed from the record lengths of 450 s. The S6N18 site was located about 150 km far from the epicenter of the 2020b event.

COMPARISON OF VERTICAL COMPONENT PEAK AMPLITUDES OF P- AND S-WAVES: K-/KIK-NET VERSUS S-NET

First, the comparison of the PGA and PGV for the P-wave parts of the vertical components are discussed. The peak values were obtained from the 5 s window starting from the P-wave onset. The values are plotted as a function of hypocentral distance in Figure 4. There are six panels in Figure 4, identified as panels A, B, C, D, E, and F. The panels A, B, and C show the plots for the PGAs for the 2018, 2020a, and 2020b events, respectively (see Data and methods section for the description of the events). Similarly, the panels D, E, and F show the plots for the PGVs for the three events, respectively. In the plots, it can be seen that the values at the land sites (circles) are noticeably larger than those at the S-net ocean bottom sites (triangles) at the comparable distances in the average sense. The higher values at the land sites may be explained by the relatively lower P-wave velocity for the shallow sediment layers and the free surface effects. In addition, the multiple reflections of the P-waves in the water layer can produce notches at some frequencies leading to lower P-wave amplitudes, especially around the resonant frequency of P waves in the water layer (e.g., Crouse and Quilter 1991, Boore and Smith 1999, Hongqi et al. 2014). As the P waves propagate through the water layer, the amplitudes of the P waves at the sea surface can be expected to be larger than those at the seafloor.

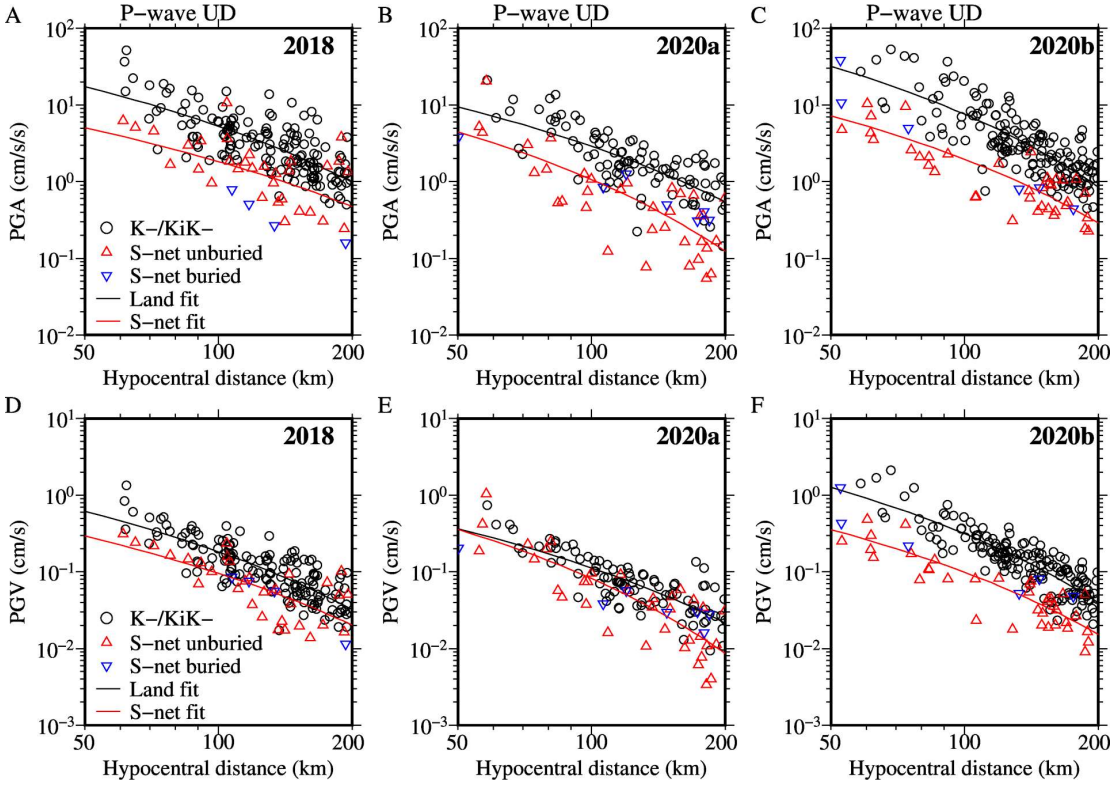

Figure 4 Plots of the PGAs (A, B, C) and PGVs (D, E, F) as a function of hypocentral distance for the 5 s window P-wave parts for the 2018, 2020a, and 2020b events respectively. The circles denote the values at the K-NET/KiK-net stations, simply written as Land in the legends, and the triangles S-net stations of which the inverse triangles (blue colored) denote the buried (about 1 m) stations, while the normal triangles denote the non-buried stations. The

black and red solid lines represent the fitted lines between the observed values and hypocentral distances for the K-NET/KiK-net and S-net stations, respectively, in each panel.

Here, the comparison of the PGAs and PGVs for the S-wave parts of the vertical components of ground and ocean-bottom motions are discussed. The peak values were obtained from the 20 s window starting from the S-wave onset. The values are plotted as a function of hypocentral distance in Figure 5. There are six panels in Figure 5 plotted in the same manner as in Figure 4. The panels A, B, and C show the plots for the PGAs for the 2018, 2020a, and 2020b events, respectively (see Data and methods section for the description of the events). Similarly, the panels D, E, and F show the plots for the PGVs for the three events, respectively. In the plots, it can be seen that the values at the land sites (circles) are somewhat larger than or similar to those at the S-net ocean bottom sites (triangles) at the comparable distances in the average sense. The relatively smaller difference for the S-wave parts may be explained by that the vertical component S-wave windows mainly consists of S waves at the ocean bottom, which are less or not influenced by the water layer above.

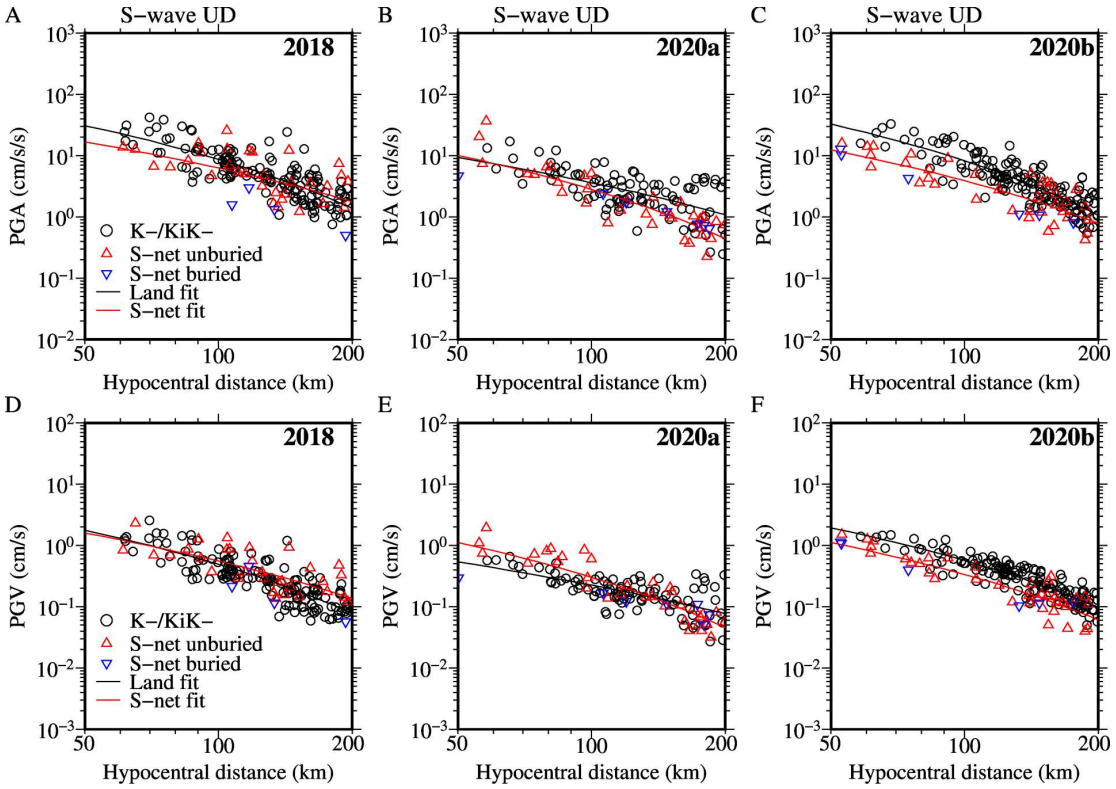

Figure 5 Same as Figure 4, but for the S-wave parts (20 s window starting from the S-wave onset) of the vertical components of recorded motions.

COMPARISON OF HORIZONTAL COMPONENT PEAK AMPLITUDES OF P AND S WAVES: K-/KIK-NET VERSUS S-NET

Here, the comparison of the PGAs and PGVs for the S-wave parts of the horizontal components of ground and ocean-bottom motions are discussed. The peak values were obtained from the 20 s window starting from the S-wave onset similar to that described in the previous section. The larger peak value between the two horizontal components is considered to be the peak value in the present analysis. The values are plotted as a function of hypocentral distance in Figure 6. There are six panels in Figure 6 plotted in the same manner as in Figures 4 and 5. The panels A, B, and C show the plots for the PGAs for the 2018, 2020a, and 2020b events, respectively (see Data and methods section for the description of the events). Similarly, the panels D, E, and F show the plots for the PGVs for the three events, respectively. In the plots, it can be seen that the values at the land sites (circles) are on average smaller than those at the S-net ocean bottom sites (triangles) at the comparable distances for the 2018 and 2020a events. These results are in contrast to those discussed in Figures 4 and 5 for the P wave parts and S wave parts on the vertical components. The larger amplification of horizontal components of motions at the seafloor can explain the difference. But the similar trends between the two sets of data for the 2020b event for the horizontal components are interesting and need further analysis.

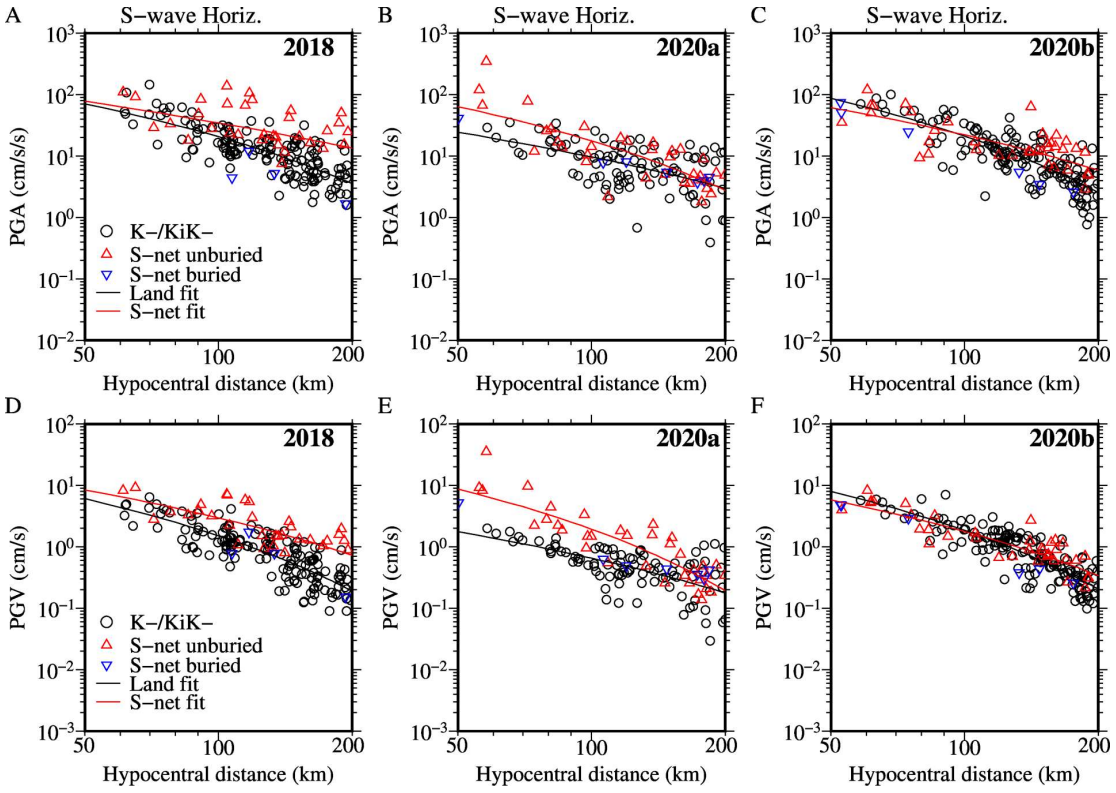

Figure 6 Plots of the PGAs (A, B, C) and PGVs (D, E, F) as a function of hypocentral distance for the 20 s window of horizontal components of S-wave parts for the 2018, 2020a, and 2020b events respectively. The circles denote the values at the K-NET/KiK-net stations, simply written as Land in the legends, and the triangles S-net stations of which the inverse triangles (blue colored) denote the buried (about 1 m) stations, while the normal triangles denote the non-buried stations. The black and red solid lines represent the fitted lines between the observed values and hypocentral distances for the K-NET/KiK-net and S-net stations, respectively, in each panel.

COMPARISON OF HORIZONTAL & VERTICAL COMPONENT PEAK AMPLITUDES BASED ON LONG-DURATION RECORDS: S-NET VS MESO-NET (0.1-0.5 HZ)

In this section, the comparison of the peak values at the S-net and MeSO-net sites are discussed. See the Data and methods section for the description of the networks and the data. The comparison was done for the PGAs obtained from the 0.1 to 0.5 Hz bandpass-filtered records of length 450 s, starting from the earthquake origin time. The PGAs are plotted for the radial (RD), transverse (TR) and vertical components of motions for the events 2018 (A, B, C), 2020a (D,E,F) and 2020b (G, H, I), respectively. As the deep sediments significantly influence the low-frequency motions, the PGA values plotted in the figures are color-coded by the depths to the layer having Vs value of 1.4 km/s (hereafter abbreviated as D14) beneath the sites. The D14 values were taken from the subsurface velocity model available at Japan Seismic Hazard Information Station (J-SHIS) (Fujiwara et al. 2012). The D14 was the suitable parameter to reduce the errors of the GMPEs for long periods (1 - 10 s) in Morikawa and Fujiwara (2013) and Dhakal et al. (2015). The D14 values are distributed over a relatively narrow depth range, but mostly deeper, for the S-net sites compared to those for the MeSO-net sites. The plots show that the PGAs were noticeably smaller at sites having D14 values smaller than about 100 m at the MeSO-net sites. The PGAs were generally larger at the S-net sites than the MeSO-net sites at equal distances, on average. However, in the plots (G, H, I), it can be seen that the differences between the S-net and MeSO-net stations were smaller for the 2020b event for all the three components. These results for the low-frequency (0.1-0.5 Hz) motions for these three events are generally similar to those discussed in Figure 6 for the horizontal components of S waves. On the other hand, the low-frequency vertical components of motions are nearly opposite to that plotted in Figures 4 and 5 for the P- and S-wave parts of the unfiltered vertical components, suggesting that the low-frequency vertical components of motions can be as strong as those on land or even stronger at the seafloor sites.

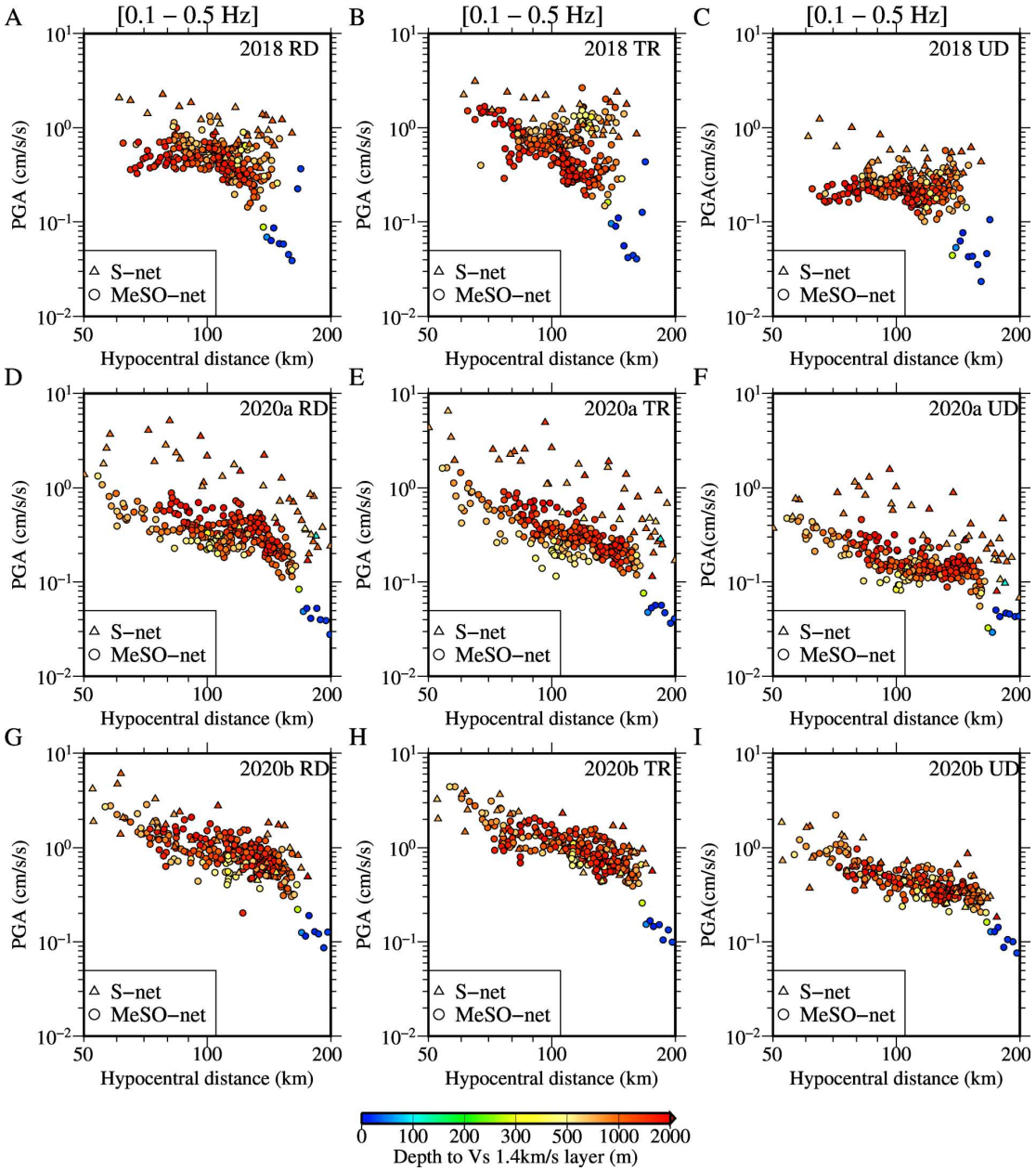

Figure 7 Plots of the PGAs for the radial (RD), transverse (TR) and vertical components of motions for the events 2018 (A, B, C), 2020a (D,E,F) and 2020b (G, H, I), respectively. The values were obtained from the 0.1 to 0.5 Hz bandpass-filtered records of length 450 s starting from the earthquake origin time. The triangles denote the S-net stations and the circles MeSO-net stations. See the Data and methods section for the description about the MeSO-net stations. The values plotted in the figures are colored by the corresponding depths in meter to the layer having Vs value of 1.4 km/s. The depth values were taken from the subsurface velocity model available at Japan Seismic Hazard Information Station (J-SHIS) (Fujiwara et al. 2012).

CONCLUSIONS

Peak values of the strong-motion records were analyzed at the S-net ocean-bottom seismograph sites located close to the Kanto basin and at the K-NET/KiK-net surface sites and MeSO-net borehole sites located in and around the Kanto Basin for three nearby earthquakes of comparable magnitudes (Mw 5.8 - 5.9) but differing in tectonic types and focal depths. The horizontal component PGAs and PGVs for the intraslab and interplate events were, on average, larger at the S-net ocean bottom sites than those at the K-NET/KiK-net land sites. The results were generally expected considering the wide presence of lower Vs values for the subsea sediments and higher Q value in the Pacific Plate. On the other hand, the vertical component PGAs and PGVs from P-wave parts were generally smaller at the S-net sites than those at the K-NET/KiK-net sites for all the events, even though the difference was less conspicuous for the PGVs. These results are also expected as the water layer makes the ocean bottom sites equivalent to the borehole sites on the land for the P-waves, causing a reduction of high-frequency amplitudes due to transmission and reflection of P-waves at the sediment-water interface. In addition, larger amplification of P waves at the land sediment sites can be expected due to lower P wave velocities in the unsaturated upper soft layers. For S-wave parts on the vertical components, the PGAs and PGVs from the crustal event were systematicaly smaller at the S-net sites than those at the K-NET/KiK-net sites, while they were either comparable or did not show the consistent difference for the other events. The PGAs computed from the 0.1 to 0.5 Hz bandpass-filtered long-duration records at the S-net sites were either comparable or larger than those at the MeSO-net sites, in contrast to those between the values for the unfiltered P waves. It is concluded that further analysis of the data considering the differences in the tectonic types of the events, propagation path, and site conditions are necessary, and the studies are in progress.

Acknowledgments

We would like to thank the Japan Meteorological Agency for providing us with hypocenter information for the earthquakes used in this study. We would also like to thank Wessel and Smith (1998) for providing us with Generic Mapping Tools, which were used to make some figures in the manuscript. This study was supported by "Advanced Earthquake and Tsunami Forecasting Technologies Project" of NIED and JSPS KAKENHI Grant Number JP20K05055.

ABSTRACT

A large-scale seafloor observation network, known as S-net, has been operated by National Research Institute for Earth Science and Disaster Resilience (NIED) in the Japan Trench area since 2016. The main objective of the observation is to provide reliable earthquake and tsunami early warnings. The network consists of 150 in-line-type observatories with sensors housed in cylindrical pressure vessels. The stations and cables were buried about one meter beneath the seafloor in the region of water depth < 1500 m while they were sited on the seafloor in the deeper area. Previous studies have shown that the S-net sensors rotate after some threshold peak ground accelerations due to poor coupling between the sensor house and sediment, resulting in large rotational noises. Another serious concern at the S-net sites is the amplification effect of sediments. To minimize the various effects, researchers have devised equations using the displacement amplitude of vertical component of motions to estimate the magnitude for Japan Meteorological Agency earthquake early warning (Hayashimoto et al. 2019). The vertical motions are affected as well by the presence of water layer in the oceanic area. Thus, the analysis of seafloor records is challenging due to the multiply effects of sediments and water layer. In this meeting, we report the results of analyses of strong-motion records at the ground in the Kanto Basin and adjoining areas and the S-net sites from nearby moderate to strong offshore earthquakes. Strong motions at ground and borehole sites were taken from K-NET/KiK-net and MeSO-net, respectively. We have found that the horizontal PGAs and PGVs at the S-net sites were, on average, similar to or larger than those at the ground and borehole sites at equal distances. In contrast, the vertical PGAs and PGVs at the S-net sites tended to be smaller than those at the ground sites for the S wave. Notably, the PGAs and PGVs for the P-wave parts on the vertical records of S-net were smaller than those at the ground sites. A portion of the results was published in Dhakal and Kunugi (2021). We are now analyzing a larger dataset and report the detailed results elsewhere. This study was supported by the "Advanced Earthquake and Tsunami Forecasting Technologies Project" of NIED and JSPS KAKENHI Grant Number JP20K05055.

REFERENCES

Aoi, S., Asano, Y., Kunugi, T., Kimura, T., Uehira, K., Takahashi, N., Ueda, H., Shiomi, K., Matsumoto, T., and Fujiwara, H. (2020). MOWLAS: NIED Observation Network for Earthquake, Tsunami and Volcano. Earth Planets Space 72, 126. doi: 10.1186/s40623-020-01250-x

Boore, D. M. and Smith, C. E. (1999). Analysis of earthquake recordings obtained from the Seafloor Earthquake Measurement System (SEMS) Instruments deployed off the coast of Southern California. Bull. Seism. Soc. Am. 89(1), 260–274.

Crouse, C. B. and Quilter, J. (1991). Seismic hazard analysis and development of design spectra for Maul A platform. Proc. Pacific Conf. on Earthquake Engineering, 20-23 Nov, New Zealand, Vol. 3, 137-148.

Dhakal, Y.P., Kunugi, T., Suzuki, W., Kimura, T., Morikawa, N., and Aoi, S. (2021). Strong motions on land and ocean bottom: comparison of horizontal PGA, PGV, and 5% damped acceleration response spectra in northeast Japan and the Japan Trench area. Bull. Seism. Soc. Am. 111 (6): 3237–3260. doi: 10.1785/0120200368

Dhakal, Y.P. and Kunugi, T. (2021) An Evaluation of Strong-Motion Parameters at the S-net Ocean-Bottom Seismograph Sites Near the Kanto Basin for Earthquake Early Warning.Front. Earth Sci. 9:699439.doi: 10.3389/feart.2021.699439

Fujiwara, H., Kawai, S., Aoi, S., Morikawa, N., Senna, S., Azuma, H., Ooi, M., Hao, K.X., Hasegawa, N., Maeda, T., Iwaki, A., Wakamatsu, K., Imoto, M., Okumura, T., Matsuyama, H., and Narita, A. (2012). Some improvements of seismic hazard assessment based on the 2011 Tohoku earthquake. Technical Note of the National Research Institute for Earth Science and Disaster Prevention, No. 379, 1-349. (in Japanese)

Hongqi, D., Hu, J., and Lili, X. (2014). Effect of seawater on incident plane P and SV waves at ocean bottom and engineering characteristics of offshore ground motion records off the coast of southern California, USA. Earthq. Eng. Eng. Vib. 13, 181–194. doi: 10.1007/s11803-014-0222-4

Kano, M., Nagao, H., Sakai, S., Nakagawa, S., Mizusako, S., Hori, M., Hirata, N., Shiomi, K., Honda, R. (2015). Azimuth verification of the MeSO-net seismographs. Zisin 68(2), 31-44. doi: 10.4294/zisin.68.31 (in Japanese with English abstract)

Nakamura, T., and Hayashimoto, N. (2019). Rotation motions of cabled ocean-bottom seismic stations during the 2011 Tohoku earthquake and their effects on magnitude estimation for early warnings. Geophys. J. Int. 216, 1413–1427. doi: 10.1093/gji/ggy502

Okada, Y., Kasahara, K., Hori, S., Obara, K., Sekiguchi, S., Fujiwara, H., and Yamamoto, A. (2004). Recent progress of seismic observation networks in Japan —Hi-net, F-net, K-NET and KiK-net—, Earth Planets Space, 56, xv-xxviii.

Sakai S., and N. Hirata (2009). Distribution of the Metropolitan Seismic Observation network. Bull. Earthq. Res. Inst. Univ. Tokyo, v84, pp. 57-69 (in Japanese with English abstract).

Takagi, R., Uchida, N., Nakayama, T., Azuma, R., Ishigami, A., Okada, T., Nakamura, T., and Shiomi, K. (2019). Estimation of the orientations of the S-net cabled ocean-bottom sensors. Seismol. Res. Lett. 90, 2175-2187. doi: 10.1785/0220190093

Wessel, P., and Smith, W.H.F. (1998). New, improved version of generic mapping tools released. Eos, Transactions, American Geophysical Union, 79, 579. doi: 10.1029/98EO00426